

Unusual magnetostriction behavior and magnetoelectric effect in spinel MnV_2O_4

Qing-Yuan Liu¹, Yinina Ma,² Young Sun,² Zi-Yi Liu,^{1,2} Jin-Guang Cheng^{1,2}, Xue-Bo Zhou,^{1,2} Lei Tao,³ Ming-Xue Huo,^{3,*} Xian-Jie Wang,^{1,†} and Yu Sui^{1,3,‡}

¹*School of Physics, Harbin Institute of Technology, Harbin 150001, China*

²*Beijing National Laboratory for Condensed Matter Physics and Institute of Physics, Chinese Academy of Sciences, Beijing 100190, China*

³*Laboratory for Space Environment and Physical Sciences, Harbin Institute of Technology, Harbin 150001, China*

 (Received 14 June 2020; revised 5 September 2020; accepted 16 September 2020; published 2 October 2020)

We investigated the magnetostriction behaviors and magnetoelectric effect of spinel structured MnV_2O_4 using the magnetization, thermal expansion, magnetostriction, permittivity, and pyroelectricity measurements. Two successive transitions were observed at T_S and T^* in all measurements. The weak electric polarization begins to appear below T_S , and can be suppressed noticeably by applying a magnetic field below T^* , indicative of the obvious magnetoelectric effect in MnV_2O_4 . Furthermore, MnV_2O_4 exhibits large low-field magnetostriction up to 6000 ppm at 7 kOe between T^* and T_S . Except for the strain at the structural transition T_S , MnV_2O_4 also shows another large strain at T^* under the magnetic field, originating from the rearrangement of tetragonal domains. Decreasing temperature allows the easy magnetization axis of MnV_2O_4 to rotate from parallel to the ab_T plane to parallel to the c_T axis because of the disappearance of weak orbital fluctuations at T^* , which leads to the rearrangement of tetragonal domains at T^* under the magnetic field.

DOI: [10.1103/PhysRevB.102.144404](https://doi.org/10.1103/PhysRevB.102.144404)

I. INTRODUCTION

Multiferroic materials are at the forefront of contemporary research areas due to the great promise in practical applications [1,2], and usually exhibit coupling of different types of ferroic orders, including ferroelasticity, ferroelectricity, and ferromagnetism [3,4]. Magnetostriction is fundamental to the coupling process in multiferroic materials, although it is still an open question on the issue of the correlation between structure, magnetic order, and ferroelectricity [5]. The interplay between lattice, spin, orbital, and charge has been widely observed in frustrated spinel oxides [6]. Magnetically driven ferroelectricity of a few different types, such as spin-canting-induced ferroelectricity in FeV_2O_4 [7], ferroelectricity derived from conical magnetic structures in CoCr_2O_4 [8], and MnCr_2O_4 [9], and $\uparrow\uparrow\downarrow\downarrow$ spin ordering in CdV_2O_4 [10], are notable reports for this kind of interplay. Besides, ferroelectricity was found in the collinear ferrimagnetic state of CoCr_2O_4 [11].

Similar to FeV_2O_4 , MnV_2O_4 with a normal spinel structure exhibits a noncollinear ferrimagnetic structure, and was also considered as a candidate for multiferroic materials [12]. Though no ferroelectricity was reported in MnV_2O_4 , large magnetodielectric response and magnetostriction below magnetic ordering temperature were already discovered [13–17], suggesting the existence of possible magnetoelectric coupling. Further, we found that MnV_2O_4 exhibits two successive transitions at $T_S \sim 56$ K and at $T^* \sim 51$ K, respectively, which

are associated to the change in the orbital state of V^{3+} ions occupying the central position in the oxygen octahedron [18]. Although a cubic-to-tetragonal structural transition induced by the orbital ordering of V^{3+} ions occurs at T_S , a certain degree of orbital fluctuation still occurs below T_S , which are completely suppressed at T^* . Also, a noncollinear ferrimagnetic ordering transition occurs together with the structural transition at T_S . A small lattice distortion was also observed at T^* . After the structural transition from cubic to tetragonal, three types of tetragonal crystallographic domains are formed in MnV_2O_4 , as verified by the single crystal x-ray diffraction [13], transmission electron microscopy [19,20], and nuclear magnetic resonance [21]. Because of the rearrangement of tetragonal domains, MnV_2O_4 exhibits a magnetic shape-memory effect and large magnetostriction below T_S [13–15]. However, in previous reports, only one sharp drop of strain was observed at T_S [13,15,17], but there was no noticeable strain anomaly at T^* in MnV_2O_4 , which is inconsistent with the small lattice distortion at T^* . Besides, the strain observed below T_S is significantly smaller than expected for a single-domain structure under the magnetic field [13,17]. Likewise, there is still an absence of understanding about the physical origin of the arrangement of tetragonal domains in MnV_2O_4 .

Therefore, in this work, we have further studied the effects of the change in orbital state on the magnetic anisotropy, rearrangement of tetragonal domains, and electric polarization in MnV_2O_4 . The disappearance of weak orbital fluctuations at T^* can prompt the easy magnetization axis of MnV_2O_4 to rotate from the ab_T plane to the c_T axis. Due to the reorientation of the easy magnetization axis at T^* , the tetragonal domains also rearrange at T^* under the magnetic field, leading to a large strain. Besides, we discovered the polarization and obvious magnetoelectric effect in MnV_2O_4 below T_S , which

*Corresponding author: huomingxue@hit.edu.cn

†Corresponding author: wangxianjie@hit.edu.cn

‡Corresponding author: suiyu@hit.edu.cn

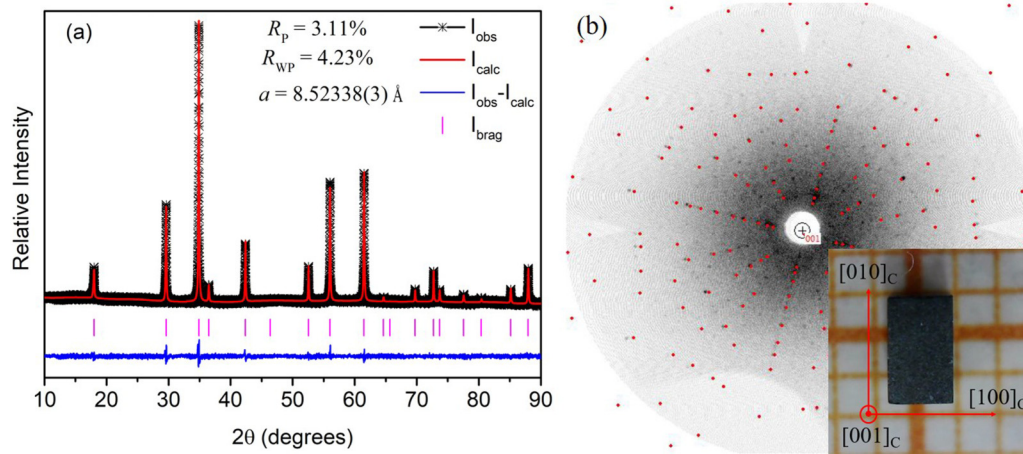


FIG. 1. (a) Room-temperature x-ray powder diffraction patterns (plus marks) and Rietveld refinement patterns (solid lines) for MnV_2O_4 . (b) Laue back diffraction pattern for the crystal oriented along the $[001]_C$ axis. Here, the subscript C represents the cubic phase. Inset of (b), the oriented crystal in the shape of a cube, in which three axial directions are marked as $[100]_C$, $[010]_C$, and $[001]_C$.

originate from the tiny deviation from the centrosymmetric $I4_1/a$ space group.

II. EXPERIMENT

MnV_2O_4 single crystals were grown by the floating zone technique [18]. The phase purity was analyzed by x-ray diffraction (XRD) and the proportion of Mn to V was checked by the induction coupled plasma (ICP) measurement. The x-ray Laue back diffraction was used to determine the crystal principal axis, and the oriented crystal was cut into cubic shape, as shown in the inset of Fig. 1(b). To facilitate the description and analysis of the following magnetic measurements along different directions, since the three axial directions are equivalent, they are defined as $[100]_C$, $[010]_C$, and $[001]_C$, respectively (the subscript C represents cubic phase).

The magnetization $M(H)$, magnetic susceptibilities $M(T)$, and rotational behaviors of the moment of the oriented samples were measured by employing a superconducting quantum interference device magnetometer. At that juncture, $M(T)$ curves were recorded, using the so-called zero field-cooled (ZFC), field-cooled-cooling (FCC), and field-cooled-warming (FCW) procedures. $M(H)$ curves along $[001]_C$ direction and rotational behaviors of the moments were recorded after a zero-field cooling from 100 K, which is far above the magnetic ordering temperature, and the rotational behaviors of the moments at different temperatures were measured at $H = 50$ Oe along the direction $[100]_C \rightarrow [001]_C \rightarrow [-100]_C \rightarrow [00-1]_C \rightarrow [100]_C$ of the sample illustrated in Fig. 1(b). The thermal expansion $\Delta L/L_{70\text{K}}$ along $[001]_C$ direction were recorded in both ZFC and FCC procedures, and magnetostrictions $\Delta L/L_0$ along the $[001]_C$ direction were recorded after a zero-field cooling from 100 K. They were all performed by using AH 2550A capacitance dilatometer that was calibrated with 99.999% pure Cu and Al rods. For an unoriented sample with dimensions of $3.9 \text{ mm} \times 3.4 \text{ mm} \times 0.5 \text{ mm}$, the dielectric permittivity measurement was performed using Agilent 4980A LCR meter in the cooling process, and the pyroelectric current was recorded with a Keithley 6517B electrometer. In

practice, the electric field E was applied at 100 K, followed by cooling down to 10 K and subsequent measurement of the current I_P upon warming up to 70 K at a rate of 5 K/min. The magnetic field H was kept parallel to the electric field E or the direction of the electrode (when $E = 0$ V/m). In the above-mentioned measurements, the temperature and the magnetic field were controlled by the physical property measurement system.

III. RESULTS

The Rietveld analysis of the powder diffraction pattern of MnV_2O_4 at room-temperature is shown in Fig. 1(a). It indicates a single phase with a cubic structure ($Fd-3m$). The lattice parameter obtained from the Rietveld refinements is $a = 8.52338(3) \text{ \AA}$, which is very close to those reported for the MnV_2O_4 ceramics ($8.5210(2) \text{ \AA}$ [22], $8.52545(5) \text{ \AA}$ [23]), and significantly larger than the lattice parameter of the single crystal sample reported before ($8.5063(2) \text{ \AA}$) [22]. In previous literature, the lattice parameter of MnV_2O_4 single crystal is typically smaller than that of polycrystalline samples [22,23], because the vanadium deficiency is easily formed in the crystal due to the evaporation of vanadium during the growth of single crystals. These results suggest that nearly stoichiometric MnV_2O_4 single crystals were grown, which was further verified by the ICP measurement showing that the average Mn:V atomic ratio is 1.03:1.97. The Laue back diffraction pattern in Fig. 1(b) shows that crystal orientation is along the $[001]_C$ direction.

The anisotropic magnetic susceptibilities of MnV_2O_4 crystal parallel to the $[001]_C$ and $[100]_C$ directions are displayed in Fig. 2(a). Two sharp peaks were observed at T_S and T^* , indicative of two successive magnetic transitions at low temperatures. It is worth noting that an obvious magnetic anisotropy is present as the temperature goes below T_S . Above T^* , the magnetic susceptibility along the $[001]_C$ direction is smaller than that along the $[100]_C$ direction, while the situation is just in reverse below T^* . As shown in Fig. 2(b), accompanied by these two magnetic transitions, the relative dielectric constant $\varepsilon(T)$ drops steeply at T_S and

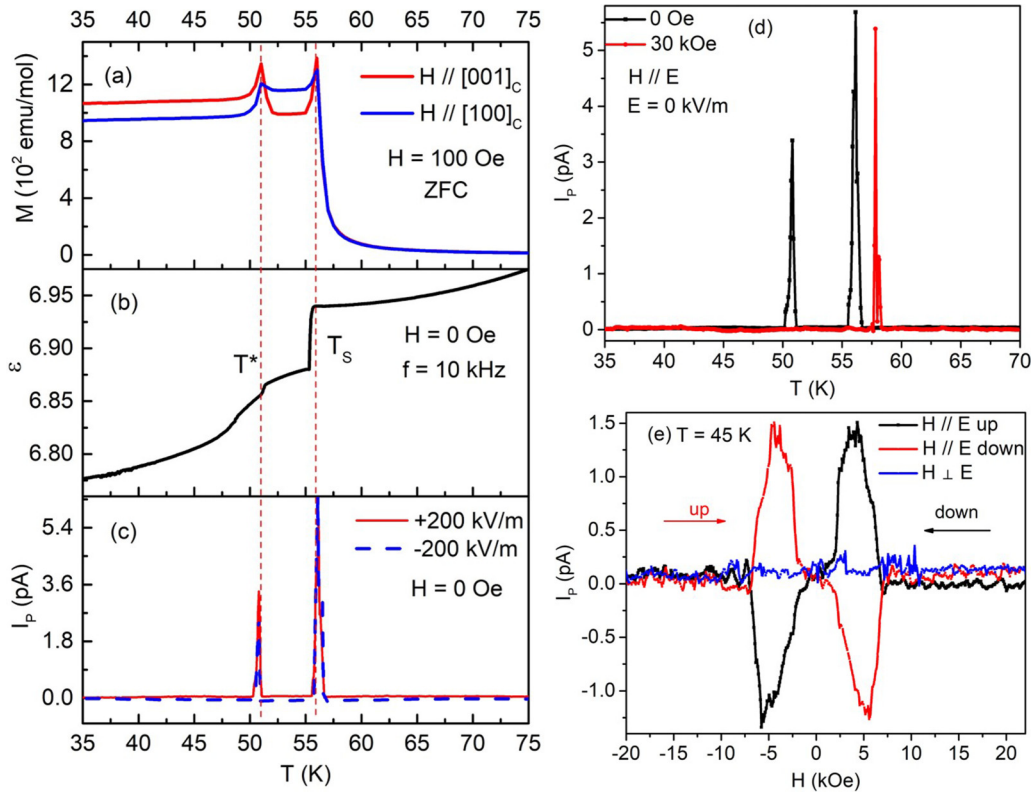


FIG. 2. (a) The anisotropic magnetic susceptibilities of MnV_2O_4 single crystal parallel to the $[001]_c$ and $[100]_c$ directions under $H = 100$ Oe in ZFC process. (b) The relative dielectric constant under $H = 0$ Oe during the cooling process. (c) The pyroelectric currents at polarization electric fields $E = \pm 200$ kV/m under zero magnetic field during the warming process. (d) The pyroelectric currents under different magnetic fields. The magnetic field H is parallel to the direction of the electrode when $E = 0$ kV/m. (e) The magnetoelectric current with $H//E$ and $H \perp E$. Here, the red (black) arrow represents that the sweep process is up to plus (up to minus).

exhibits a weak anomaly near T^* under zero field. For the meantime, the pyroelectric current exhibits two sharp peaks at T_S and T^* under zero magnetic field in Fig. 2(c), proving the spontaneous electric polarization in MnV_2O_4 related to these magnetic transitions. Yet, the pyroelectric current does not depend on the poling electric field E . This indicates that the electric polarization is not switchable. Accordingly, MnV_2O_4 can be characterized as pyroelectric rather than ferroelectric, although the magnetic ordering and polarization occur simultaneously. The simultaneous occurrence of these phenomena was also observed in pyroelectric $\text{CaBaCo}_4\text{O}_7$ [24,25], whose electric polarization upon ferrimagnetic ordering results from the strong exchange striction. Also, as shown in Fig. 2(d), the peak of the pyroelectric current at T^* disappears under $H = 30$ kOe, which asserts the magnetoelectric effect of MnV_2O_4 since the electric polarization can be regulated by the magnetic field. With an increasing magnetic field, the electric polarization would be inhibited, as shown in Figs. S1(a) and S1(b) of the Supplemental Material [26].

The spin-canting-induced ferroelectricity was found in FeV_2O_4 [7], which exhibits a similar noncollinear ferrimagnetic structure to MnV_2O_4 below T_S [18,27]. However, if the electric polarization in MnV_2O_4 is induced by the noncollinear magnetic structure, theoretically, a switchable electric polarization should be observed in MnV_2O_4 , just as found in FeV_2O_4 [7]. Besides, based on this hypothesis, there will be no pyroelectric current peak at T^* , since that

the noncollinear magnetic structure of MnV_2O_4 begins to appear at T_S . But in Fig. 2(c), MnV_2O_4 shows a nonswitchable electric polarization and two pyroelectricity current peaks below T_S , contradicting the analyses above. Hence, the mechanism of spin-canting-induced ferroelectricity in FeV_2O_4 is not appropriate for MnV_2O_4 . It is worth noticing that the magnetoelectric effect in MnV_2O_4 occurs only for $H//E$ (the direction of the electrode), as shown in Fig. 2(e). A similar phenomenon was reported for CoCr_2O_4 having a collinear ferrimagnetic structure [11], wherein a noncentrosymmetric tetragonal structure was assumed to be induced by magnetostriction, and then generated the polarization P parallel to its magnetization M . Consequently, the electric polarization in MnV_2O_4 may well be also closely related to exchange striction.

To further verify the origin of the pyroelectric polarization observed in MnV_2O_4 , the temperature dependence of thermal expansion ($\Delta L/L_{70\text{K}}$) of the MnV_2O_4 crystal along the $[001]_c$ direction was estimated in ZFC and FCC processes under different magnetic fields ($H//L$), where the value of $\Delta L/L_{70\text{K}}$ was normalized as $[L(T) - L(70\text{K})]/L(70\text{K})$. As displayed in Fig. 3(a), the value of $\Delta L/L_{70\text{K}}$ decreases steeply at ~ 55.5 K under zero field, once again proving that a structural phase transition occurs at T_S . But only an insignificant salutation of $\Delta L/L_{70\text{K}}$ can be observed at $T^* \sim 51.5$ K, which is very close to the peak temperature of magnetic susceptibility. On the other hand, the temperature dependence of

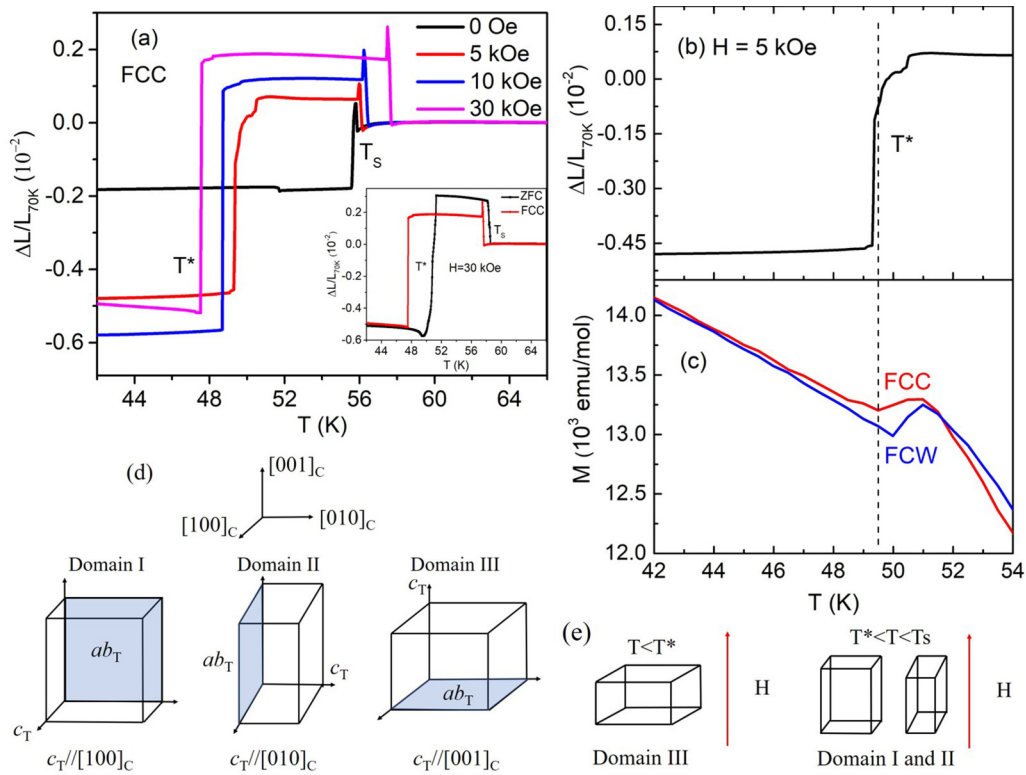


FIG. 3. (a) The thermal expansion of MnV_2O_4 single crystal along the direction $[001]_C$ under different magnetic fields ($H//L$) in the FCC process. Inset of (a), the thermal expansion under $H = 30\text{ kOe}$ in ZFC and FCC processes. (b) and (c) The temperature dependence of thermal expansion (in the FCC process) and magnetic susceptibility (in FCC and FCW process) of MnV_2O_4 single crystal under $H = 5\text{ kOe}$, respectively. (d) The schematic graphic of the three tetragonal domains below T_S . (e) The c_T axis is parallel to the magnetic field below T^* , while it is perpendicular to the magnetic field between T^* and T_S .

$\Delta L/L_{70\text{K}}$ is reversed under the magnetic field (even only 5 kOe), showing a sharp increase at T_S and then a sudden drop at T^* . It is very strange that such a small magnetic field can induce such immense influence on these two transitions. As the magnetic field increases, the T_S gradually moves toward higher temperatures, while T^* gradually moves toward lower temperatures. Meanwhile, as shown in Figs. 3(b) and 3(c), a sharp decline in magnetic susceptibility with an evident thermal hysteresis occurred at T^* , suggestive of the first-order nature of this transition. Thermal hysteresis was also observed in the thermal expansion curves shown in Fig. 3(a).

In the tetragonal phase of MnV_2O_4 , three different types of tetragonal domains are formed in the MnV_2O_4 crystal after the structure changes from the cubic phase into the tetragonal phase at T_S , just as shown in Fig. 3(d). They are marked as domains I, II, and III, respectively, with the c_T axis parallel to the $[100]_C$, $[010]_C$, and $[001]_C$ directions. Here, the subscript T represents the tetragonal phase. Compared with the cubic phase, the tetragonal phase contracts along the c_T axis but expands in the ab_T plane ($c_T = 8.459\text{ \AA} < a_C = 8.513\text{ \AA}$, $\sqrt{2}a_T = 8.540\text{ \AA} > a_C = 8.513\text{ \AA}$) [18]. In view of the condition where only the single tetragonal domain III exists in MnV_2O_4 crystal, having the c_T axis parallel to the test direction L , the value of $\Delta L/L_{70\text{K}}$ along the c_T axis should be about $(c_T - a_C)/a_C = -0.63\%$ in the tetragonal phase in accordance with the relative change in the lattice parameter after the structural transition. On the contrary, the maximum

value of $\Delta L/L_{70\text{K}}$ is about $(\sqrt{2}a_T - a_C)/a_C = 0.32\%$ in the case where only domains I or II exist in the crystal, having their c_T axis perpendicular to the test direction L .

The value of $\Delta L/L_{70\text{K}}$ in our MnV_2O_4 crystal is only about -0.2% below T_S under zero field, which is close to the value of -0.15% reported by Suzuki *et al.* [13, 17], but is greatly different from the theoretical value of -0.63% estimated above. It is our assumption that this distinction could originate from the partial random orientation of the three tetragonal domains under zero field. Under $H = 30\text{ kOe}$, the $\Delta L/L_{70\text{K}}$ increases sharply to $\sim 0.2\%$ at T_S as shown in Fig. 3(a), which is close to the theoretical value of 0.32% . That is, primarily there exists either domain I or domain II under a strong magnetic field between T^* and T_S . Nonetheless, contrary to the behavior of $\Delta L/L_{70\text{K}}$ at T_S , a large contraction of L is observed at T^* under the magnetic field. The $\Delta L/L_{70\text{K}}$ undergoes a reduction of about $-0.5\% \sim -0.6\%$ below T^* compared to that in the cubic phase, which is almost equal to the theoretical value of -0.63% for the existence of only single domain III. In other words, under the magnetic field and below the temperature T^* , only single domain III is present in MnV_2O_4 crystal, in which the c_T axis is parallel to $H(H//L)$. Nevertheless, the domains I and II exist above T^* whose c_T axis are perpendicular to H under high field. This observation implies that the tetragonal domains undergo a rotation by 90° from domain I or domain II to domain III at T^* . And so, the transition at T^* should

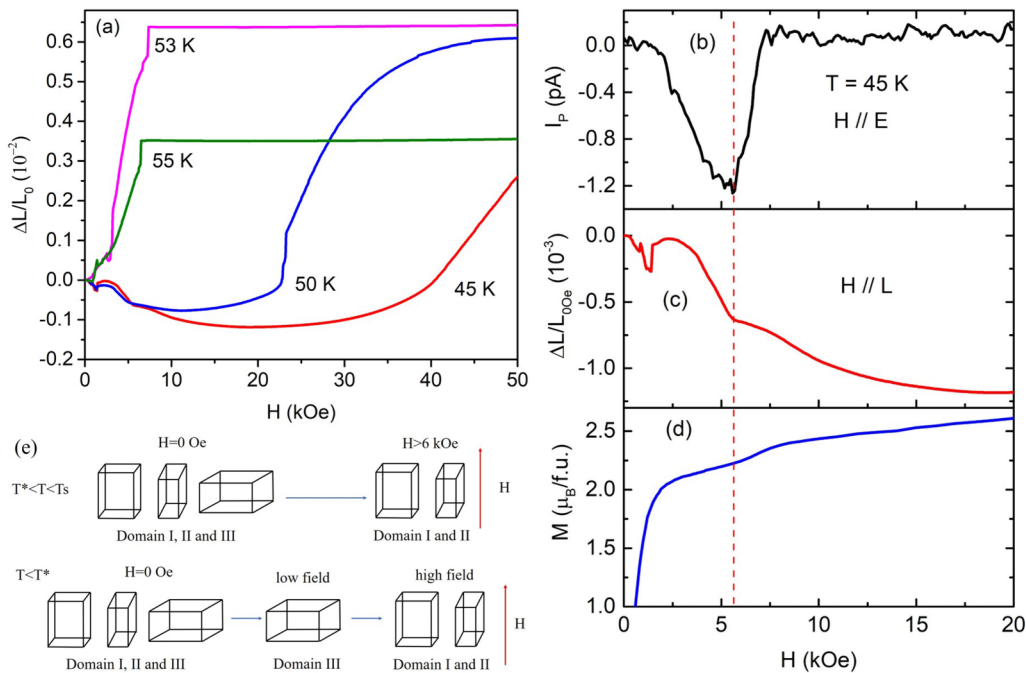


FIG. 4. (a) The initial magnetostriction of MnV_2O_4 single crystal along the direction $[001]_C$ at different temperatures. (b)–(d) The polarization current, magnetostriction curve, and $M(H)$ curve at $T = 45$ K, respectively. (e) The schematic graphic of the tetragonal domains rotating under the magnetic field. The three tetragonal domains are randomly oriented under zero field. Domains I and II are more stable under the magnetic field above T^* . Below T^* , the domain III is more stable under low field, but domains I and II reappear under high field.

come from the rearrangement of tetragonal domains under the magnetic field.

The initial magnetostriction ($H//L$) values for MnV_2O_4 crystal at different temperatures are given in Fig. 4(a), wherein the value of the $\Delta L/L_0$ is normalized as $[L(H) - L(0\text{Oe})]/L(0\text{Oe})$. To avoid the effect of magnetic history on the test, the sample was cooled from 100 K under zero field before each test, which implies that the three tetragonal domains are randomly oriented under zero field. There are two key features in these magnetostriction curves. Above $T^* \sim 51$ K, the value of $\Delta L/L_0$ goes up rapidly and approaches saturation up to 6000 ppm under $H > 7$ kOe. The large magnetostriction should be also caused by the rearrangement of tetragonal domains due to the strong spin-lattice coupling, that is, the transformation of randomly oriented tetragonal domains at zero field into ordered domains I and II under high field between T^* and T_S . In contrast, below $T^* \sim 51$ K, the $\Delta L/L_0$ initially decreases and exhibits an inflection point at 6 kOe, and then slowly reduces until 20 kOe at $T = 45$ K (11 kOe at $T = 50$ K). Subsequently, it shows a rapid increase above 40 kOe at $T = 45$ K (22 kOe at $T = 50$ K). According to the data of above thermal expansion, a small amount of contraction would come up when randomly oriented tetragonal domains transform into single tetragonal domain III below T^* under a low magnetic field. Nevertheless, as evident from Fig. 3(a), T^* gradually moves toward low temperature as the field increases, which implies domain I and II are more stable under the high field. Therefore, a strong enough magnetic field could transform domain III into the domains I and II, causing a rapid increase in $\Delta L/L_0$ under the high field. Further on, we performed the measurements on magnetoelectric polarization current and magnetization $M(H)$, as illustrated in Figs. 4(b)

and 4(d), respectively. There is an apparent magnetization platform in the $M(H)$ curve and a negative peak in the pyroelectric current near 6 kOe at $T = 45$ K, indicating that the pyroelectric polarization is closely associated with the magnetostriction.

It is worth noticing that, the results regarding the thermal expansion and magnetostriction of MnV_2O_4 obtained by us are very different from those reported previously [13,15,17]. First, only one large contraction was observed below T_S under different fields in the past, but we found that the magnetic field not only can change the strain at T_S from contraction to expansion but can also cause a very large contraction at T^* . Secondly, Suzuki *et al.* pointed out that the rearrangement of tetragonal domains can cause negative magnetostriction as a result of the gradual transformation from partially random orientation domains to single domain III with increasing magnetic field [13]. It implies that domain III is more stable under the magnetic field. However, we found that domains I and II are more stable between T^* and T_S , and lead to positive magnetostriction at T_S . As a result, in addition to the magnetic field, the tetragonal domains are also susceptible to realignment at T^* with decreasing temperature. The reason for domain rearrangement at T^* is discussed in the next section. As shown in Fig. 5, according to the thermal expansion and magnetostriction data, we obtained a T - H phase diagram to illustrate the transformations in the arrangement of tetragonal domains in MnV_2O_4 with variations in temperature and magnetic field. Under low field ($H < 6$ kOe), all the three tetragonal domains coexist randomly. With an increasing magnetic field, either domain I or domain II exists between T_S and T^* , which transforms into domain III at T^* with decreasing temperature. Similar T - H phase diagrams have been

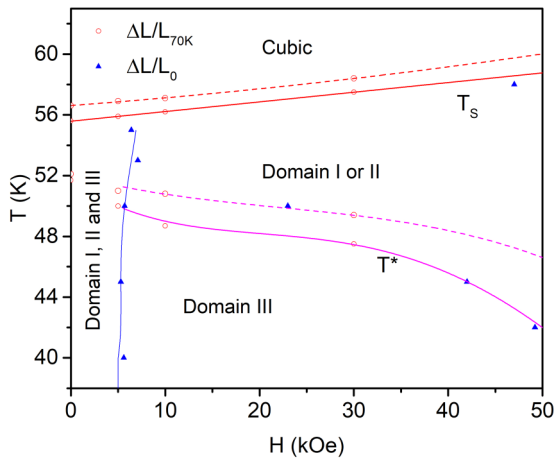


FIG. 5. The T - H phase diagram on the tetragonal domain arrangement of MnV_2O_4 derived from the thermal expansion and magnetostriction data. The red open circles represent the transition temperatures T_S and T^* , according to the thermal expansion measurement results. The blue solid triangles are the transition magnetic fields based on the magnetostriction curves. The color lines represent the phase boundaries, where the solid (dotted) line represents the cooling (warming) process. Three tetragonal domains coexist with each other under low field. With increasing magnetic field, tetragonal domains are rearranged orderly, where they are mainly domain I or domain II between T^* and T_S , and domain III below T^* .

given in Refs. [23,28], but our phase diagram focuses more on the change of the arrangement state of the three tetragonal domains in MnV_2O_4 crystal with temperature and magnetic field. Myung-Whun *et al.* speculated that the transition at T^* arises from the transformation of orbital ordering to orbital fluctuations with decrease in temperature, but our results indicate the exact opposite, i.e., the transition takes place from orbital fluctuations to orbital ordering at T^* . Hardy *et al.* mentioned that the transition at a lower temperature under the magnetic field could be relative to the rearrangement of tetragonal domains, but no detailed information was provided regarding the arrangement of the tetragonal domains. In the present work, we clearly illustrated the arrangement state of the three tetragonal domains at different temperatures and magnetic fields, in which the tetragonal domains transform from domains I and II to the domain III at T^* as the temperature decreases. The relation between the orbital fluctuations and the transformation of the tetragonal domains is discussed in the following section.

IV. DISCUSSION

Although MnV_2O_4 exhibits a cubic-to-tetragonal structural transition due to orbital ordering at T_S , we observed that a certain degree of orbital fluctuation still exists between T_S and T^* [18]. When further orbital ordering occurs at T^* , MnV_2O_4 displays a magnetic transition as well as a lattice distortion due to the interplay between spin, lattice, and orbital. But according to the above discussions, the nature of the transition at T^* is closely related to the rearrangement of tetragonal domains. Hence, there must be some relation between the

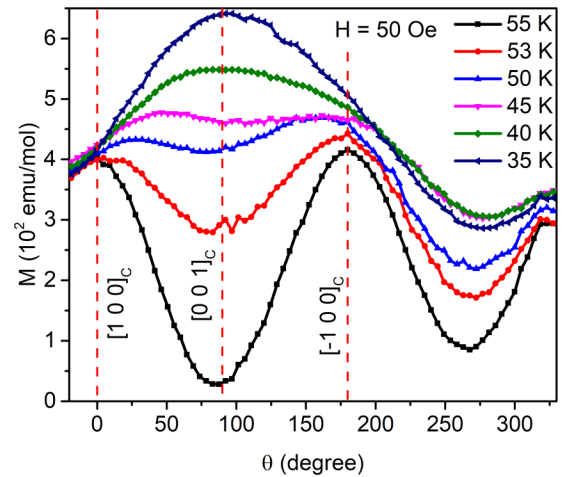


FIG. 6. The rotational behavior of the total moment in MnV_2O_4 single crystal under $H = 50$ Oe at different temperatures, which were measured along the directions $[100]_C \rightarrow [001]_C \rightarrow [-100]_C \rightarrow [00-1]_C \rightarrow [100]_C$ of the sample in illustration of Fig. 1(b).

reorientation of the tetragonal domain and the orbital fluctuations.

The rearrangement of tetragonal domains induced by magnetic field originates typically from spin-lattice coupling, because the easy axis of the tetragonal domains favors a position parallel to the field direction to minimize magnetocrystalline anisotropy energy [29]. Based on the above thermal expansion results, the c_T axis can be considered as the easy magnetization axis below T^* , but above it, the easy axis should be parallel to the ab_T plane. To further illustrate this fact, the rotational behaviors of the total moment at different temperatures are displayed in Fig. 6, which were measured along the direction sequence $[100]_C \rightarrow [001]_C \rightarrow [-100]_C \rightarrow [00-1]_C \rightarrow [100]_C$. Above $T^* \sim 51$ K, the magnetization exhibits a maximum value along the direction $[100]_C$ and a minimum value along the direction $[001]_C$, indicative of the fact that the direction $[100]_C$ is the easy magnetization axis above T^* . With the decrease in temperature, the magnetization along the direction $[001]_C$ increases gradually and attains its maximum value far below T^* , which suggests that the direction $[001]_C$ is the easy magnetization axis below T^* . Therefore, the results in Fig. 6 prove that the easy magnetization axis rotates by 90° from the $[100]_C$ to the $[001]_C$ direction at T^* . The anisotropic magnetic susceptibilities along the $[001]_C$ and $[100]_C$ directions further testified the rotation of the easy magnetization axis, as shown in Fig. 2(a).

The rotation of the easy magnetization axis was also reported for FeV_2O_4 [30], wherein it was considered to be caused by the change in the orbital state of Fe^{2+} ions. Therefore, it is essential to further analyze the correlation between the orbital state of V^{3+} ions and the rotation of the easy magnetization axis in MnV_2O_4 . In the MnV_2O_4 crystal, provided the antiferro-orbital ordering is perfect, the easy magnetization axis should be the c_T axis. But, the orbital angular momentum of V^{3+} ions are not totally quenched due to the existing orbital fluctuations [31], which can result in the enhancement in magnetic anisotropy [13,32] or even change the easy magnetization axis. Thus, it is reasonable to believe that

the weak orbital fluctuations above T^* make the easy magnetization axis parallel to the ab_T plane. Further on, the orbital fluctuations are suppressed below T^* and so the easy magnetization axis rotates from the ab_T plane to the c_T axis. To reduce the magnetocrystalline anisotropy energy, along with the 90° rotation of the easy magnetization axis, the tetragonal domains also are rearranged at T^* under the magnetic field. However, under zero field, the magnetocrystalline anisotropy energy does not vary, and so the reorientation transition of tetragonal domains would not occur at T^* though the easy magnetization axis undergoes rotation. Therefore, no obvious strain was observed at T^* for MnV_2O_4 under zero field.

It was reported earlier that the orbital fluctuations in MnV_2O_4 can be enhanced by a magnetic field [33], which implies that enough high magnetic field can induce the rotation of the easy magnetization axis from c_T axis to ab_T plane even below $T^* \sim 51$ K. Therefore, as shown in Fig. 4(e), even below $T^* \sim 51$ K, due to the rotation of the easy magnetization axis, domain III can transform into domains I or II when the magnetic field is sufficiently high. Besides, the temperature that the strain suddenly drops can also be decreased gradually as the magnetic field increases, as displayed in Fig. 3(a).

According to the analysis presented in the previous section, the electric polarization in MnV_2O_4 is associated with the exchange striction mechanism. Previous reports on CoCr_2O_4 show that it has a centrosymmetric cubic structure, but a tiny deviation from the cubic structure was observed at collinear ferrimagnetic ordering temperature [34], which was asserted as the reason for the electric polarization at the same temperature [35]. By drawing analogy with CoCr_2O_4 in the collinear ferrimagnetic state [11], we herein make an assumption that a noncentrosymmetric tetragonal structure causes the pyroelectric current peaks at T_S and T^* in MnV_2O_4 . Though the structure of MnV_2O_4 is generally considered to be centrosymmetric (space group is $I4_1/a$ [13]) in the tetragonal phase, its structure is related to the orbital state of V^{3+} ions. For instance, the space group in MnV_2O_4 tetragonal phase may be

$I4_1/a$ (antiferro-orbital), $P4_12_12$ (orbital-Peierls), or $I4_1/amd$ (ferro-orbital) [13]. Thus, MnV_2O_4 may have a tiny deviation from space group $I4_1/a$ below T_S , because of the local symmetry breaking caused by complex orbital states. Further, the second distortion occurs at T^* due to the disappearance of the weak orbital fluctuations, which was observed by variable temperature XRD analysis [18]. Therefore, there are two pyroelectric current peaks at T^* and T_S under zero field. With an increasing magnetic field, the orbital fluctuations were further enhanced. The lattice distortion below T^* can be partially released, leading to the suppression of the pyroelectric current peak at T^* , as shown in Fig. 2(d).

V. CONCLUSIONS

In conclusion, MnV_2O_4 shows two transitions at T_S and T^* , respectively. Though the structural transition occurs at T_S , a certain degree of orbital fluctuation still exists between T_S and T^* , which disappears completely at T^* . We observed that the weak orbital fluctuations could change the magnetic anisotropy in MnV_2O_4 , wherein the easy magnetization axis is parallel to the ab_T plane between T^* and T_S , but parallel to the c_T axis below T^* . Further, the rotation of the easy magnetization axis results in the rearrangement of tetragonal domains at T^* under the magnetic field, thereby inducing a large strain at T^* . Also, the complex orbital states cause a tiny deviation from the centrosymmetric $I4_1/a$ space group in MnV_2O_4 , and lead to two noncentrosymmetric lattice distortions at T_S and T^* , which are responsible for the two pyroelectricity current peaks observed in MnV_2O_4 . Below T^* , the increasing magnetic field results in the enhancement of the orbital fluctuations, which can suppress the rearrangement of tetragonal domains and the pyroelectric current peak at T^* .

ACKNOWLEDGMENT

This work is supported by the Natural Science Foundation of China (Grants No. 51472064 and No. 51725104).

-
- [1] D. Khomskii, *Physics* **2**, 20 (2009).
 - [2] N. Hur, S. Park, P. A. Sharma, S. Guha, and S. W. Cheong, *Phys. Rev. Lett.* **93**, 107207 (2004).
 - [3] A. Bucsek, W. Nunn, B. Jalan, and R. D. James, *Phys. Rev. Appl.* **12**, 034043 (2019).
 - [4] L. I. Vergara, J. Cao, N. Rogado, Y. Q. Wang, R. P. Chaudhury, R. J. Cava, B. Lorenz, and J. L. Musfeldt, *Phys. Rev. B* **80**, 052303 (2009).
 - [5] Y. Boonyongmaneerat, M. Chmielus, D. C. Dunand, and P. Mullner, *Phys. Rev. Lett.* **99**, 247201 (2007).
 - [6] P. G. Radaelli, *New J. Phys.* **7**, 53 (2005).
 - [7] Q. Zhang, K. Singh, F. Guillou, C. Simon, Y. Breard, V. Caignaert, and V. Hardy, *Phys. Rev. B* **85**, 054405 (2012).
 - [8] Y. Yamasaki, S. Miyasaka, Y. Kaneko, J.-P. He, T. Arima, and Y. Tokura, *Phys. Rev. Lett.* **96**, 207204 (2006).
 - [9] G. T. Lin, Y. Q. Wang, X. Luo, J. Ma, H. L. Zhuang, D. Qian, L. H. Yin, F. C. Chen, J. Yan, R. R. Zhang, S. L. Zhang, W. Tong, W. H. Song, P. Tong, X. B. Zhu, and Y. P. Sun, *Phys. Rev. B* **97**, 064405 (2018).
 - [10] G. Giovannetti, A. Stroppa, S. Picozzi, D. Baldomir, V. Pardo, S. Blanco-Canosa, F. Rivadulla, S. Jodlauk, D. Niermann, J. Rohrkamp, T. Lorenz, S. Streltsov, D. I. Khomskii, and J. Hemberger, *Phys. Rev. B* **83**, 060402(R) (2011).
 - [11] S. Yang, H. X. Bao, D. Z. Xue, C. Zhou, J. H. Gao, Y. Wang, J. Q. Wang, X. P. Song, Z. B. Sun, X. B. Ren, and K. Otsuka, *J. Phys. D* **45**, 265001 (2012).
 - [12] B. Wolin, X. Wang, T. Naibert, S. L. Gleason, G. J. MacDougall, H. D. Zhou, S. L. Cooper, and R. Budakian, *Phys. Rev. Mater.* **2**, 064407 (2018).
 - [13] T. Suzuki, M. Katsumura, K. Taniguchi, T. Arima, and T. Katsufuji, *Phys. Rev. Lett.* **98**, 127203 (2007).
 - [14] K. Adachi, T. Suzuki, K. Kato, K. Osaka, M. Takata, and T. Katsufuji, *Phys. Rev. Lett.* **95**, 197202 (2005).
 - [15] Y. Nii, N. Abe, K. Taniguchi, and T. Arima, *Appl. Phys. Lett.* **100**, 051905 (2012).
 - [16] A. Kismarhardja, J. S. Brooks, H. D. Zhou, E. S. Choi, K. Matsubayashi, and Y. Uwatoko, *Phys. Rev. B* **87**, 054432 (2013).

- [17] T. Katsufujia, K. Adachia, T. Suzukia, and M. Katsumura, *Phys. B* **383**, 13 (2006).
- [18] Q. Y. Liu, Z. Y. Liu, X. B. Zhou, T. Yajima, Y. Uwatoko, J. G. Cheng, L. Tao, Z. G. Liu, M. X. Huo, X. J. Wang, and Y. Sui, *Phys. Rev. B* **100**, 224418 (2019).
- [19] Y. Murakami, T. Suzuki, Y. Nii, S. Murai, T. Arima, R. Kainuma, and D. Shindo, *Microsc.* **65**, 223 (2016).
- [20] Y. Murakami, Y. Nii, T. Arima, D. Shindo, K. Yanagisawa, and A. Tonomura, *Phys. Rev. B* **84**, 054421 (2011).
- [21] E. Jo, S. Park, J. Lee, S. Lee, J. H. Shim, T. Suzuki, and T. Katsufuji, *Sci. Rep.* **7**, 2178 (2017).
- [22] H. D. Zhou, J. Lu, and C. R. Wiebe, *Phys. Rev. B* **76**, 174403 (2007).
- [23] V. Hardy, Y. Breard, and C. Martin, *Phys. Rev. B* **78**, 024406 (2008).
- [24] R. D. Johnson, K. Cao, F. Giustino, and P. G. Radaelli, *Phys. Rev. B* **90**, 045129 (2014).
- [25] V. Caignaert, A. Maignan, K. Singh, Ch. Simon, V. Pralong, B. Raveau, J. F. Mitchell, H. Zheng, A. Huq, and L. C. Chapon, *Phys. Rev. B* **88**, 174403 (2013).
- [26] See Supplemental Material at <http://link.aps.org/supplemental/10.1103/PhysRevB.102.144404> for further information on the magnetoelectric current, the dependence on magnetic field of polarization, pyroelectricity current in cooling process, and the thermal expansions in the ZFC process of MnV_2O_4 .
- [27] K. Matsuura, H. Sagayama, A. Uehara, Y. Nii, R. Kajimoto, K. Kamazawa, K. Ikeuchi, S. Ji, N. Abe, and T. H. Arima, *Phys. Rev. Lett.* **119**, 017201 (2017).
- [28] K. Myung-Whun, J. S. Kim, T. Katsufuji, and R. K. Kremer, *Phys. Rev. B* **83**, 024403 (2011).
- [29] R. C. O'Handley, S. J. Murray, M. Marioni, H. Nembach, and S. M. Allen, *J. Appl. Phys.* **87**, 4712 (2000).
- [30] T. Katsufuji, T. Suzuki, H. Takei, M. Shingu, K. Kato, K. Osaka, M. Takata, H. Sagayama, and T. Arima, *J. Phys. Soc. Jpn.* **77**, 053708 (2008).
- [31] J. H. Chung, J. H. Kim, S. H. Lee, T. J. Sato, T. Suzuki, M. Katsumura, and T. Katsufuji, *Phys. Rev. B* **77**, 054412 (2008).
- [32] V. O. Garlea, R. Jin, D. Mandrus, B. Roessli, Q. Huang, M. Miller, A. J. Schultz, and S. E. Nagler, *Phys. Rev. Lett.* **100**, 066404 (2008).
- [33] T. Omura, T. Ishikawa, Y. Ishitsuka, and T. Katsufuji, *Phys. Rev. B* **86**, 054436 (2012).
- [34] S. Bordacs, D. Varjas, I. Kezsmarki, G. Mihaly, L. Baldassarre, A. Abouelsayed, C. A. Kuntscher, K. Ohgushi, and Y. Tokura, *Phys. Rev. Lett.* **103**, 077205 (2009).
- [35] K. Singh, A. Maignan, C. Simon, and C. Martin, *Appl. Phys. Lett.* **99**, 172903 (2011).